Program Digest, 2019 IEEE International Ultrasonics Symposium (IUS)
Glasgow, Scotland, October 6-9, 2019

Spectral peak suppression in the acoustic emissions from multiple microbubbles cavitating in focused ultrasound

Jae Hee Song
CavLab, Centre for Medical and Industrial Ultrasonics
University of Glasgow
Glasgow, UK

Paul Prentice*
CavLab, Centre for Medical and Industrial Ultrasonics
University of Glasgow
Glasgow, UK

*paul.prentice@glasgow.ac.uk

***Abstract*—Non-linear acoustic emissions from contrast agent microbubbles under focused ultrasound exposure, are often used to monitor therapeutic efficacy, and avoid long term tissue damage. We have recently reported on the mechanistic source for non-linear emissions as periodic bubble-collapse generated shock waves. In this proceeding we present a dual perspective high-speed imaging with parallel acoustic detection dataset, for the cavitation initiated from two microbubbles exposed to focused ultrasound of f_0 = 692 kHz at peak-negative pressure amplitude of 1.14 MPa. Both cavitation-bubble clouds respond in the period doubled, $f_0/2$ subharmonic shock emission regime. The cloud collapses, however, are out of phase with respect to each other, such that shocks are detected at the hydrophone at f_0. We demonstrate peak suppression in the spectrum of the combined emissions, at key frequency values.**

Keywords— microbubbles, focused ultrasound, shock wave, acoustic emissions, subharmonic, covert cavitation

I. INTRODUCTION

The acoustic emissions generated from microbubble-cavitation in the vasculature, during application of focused ultrasound for therapy, can provide important feedback on the degree of tissue damage inflicted. Many studies use features from the spectrum of the emission signal collected, to claim '*stable*' or '*inertial*' cavitation according to the desired therapeutic effect. Harmonic emissions at nf_0 (where f_0 is the frequency of the driving, and n any integer) are associated with *stable* cavitation and 'moderate' therapeutic effect, with subharmonics at nf_0/m and broadband emissions associated with inertial cavitation and 'aggressive' therapy.

We have recently reported on a study incorporating two high-speed cameras and parallel acoustic detection, as described below, to characterise the emissions from contrast agent microbubbles, flowing through a capillary and driven by focused ultrasound at f_0 = 692 kHz across relevant PNP amplitudes, [1]. The observations suggest that all non-linear emission signals may be attributed to periodic bubble-collapse generated shock waves. At lower driving PNPs, microbubble-cavitation collapses occur at the f_0 of the driving. At higher PNPs, inertia of the liquid host medium prevents collapses with each compressional phase of the driving (known as period-doubling [2]), such that shock-emission occurs at $f_0/2$.

In the spectrum of the emission signals, periodic shock waves present as peaks at frequency values determined by the emission period [3]. Accordingly, f_0 shock waves at lower PNP amplitudes generate nf_0 features at all n¸ within the sensitivity of the acoustic detector. Similarly, $f_0/2$ shock waves raise peaks at all $nf_0/2$ values. We further demonstrated that broadband emissions (over detector instrumental noise) where attributable to variations in the peak-pressure amplitudes, and the precise timings of the periodic shock emissions.

In this proceeding a further dataset is presented, for which the emission signal detected is dominated by the cavitation from two microbubbles, within the capillary at the time of focused ultrasound incidence. The cavitation from each microbubble is responding in the $f_0/2$ shock-emission regime, according to the PNP amplitude [1]. Out-of-phase period-doubled bubble-cloud collapses, however, act to suppress the $f_0/2$ subharmonic peak in the spectrum of the combined emissions, [4].

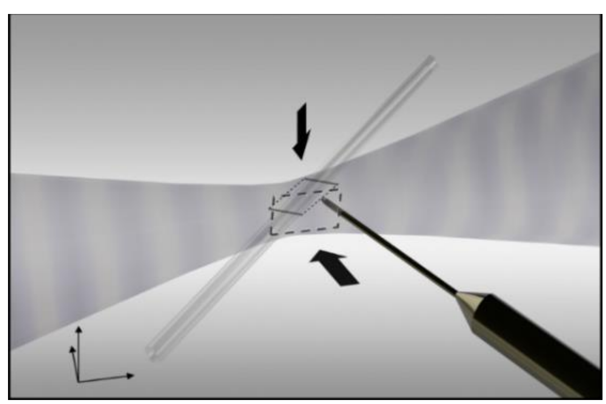

Fig. 1. Schematic representation of dual high-speed imaging and acoustic detection experimental configuration.

The research leading to these results has received funding from the European Research Council under the European Union's Seventh Framework Programme (FP/2007-2013)/ERC Grant Agreement No. 336189 (TheraCav).

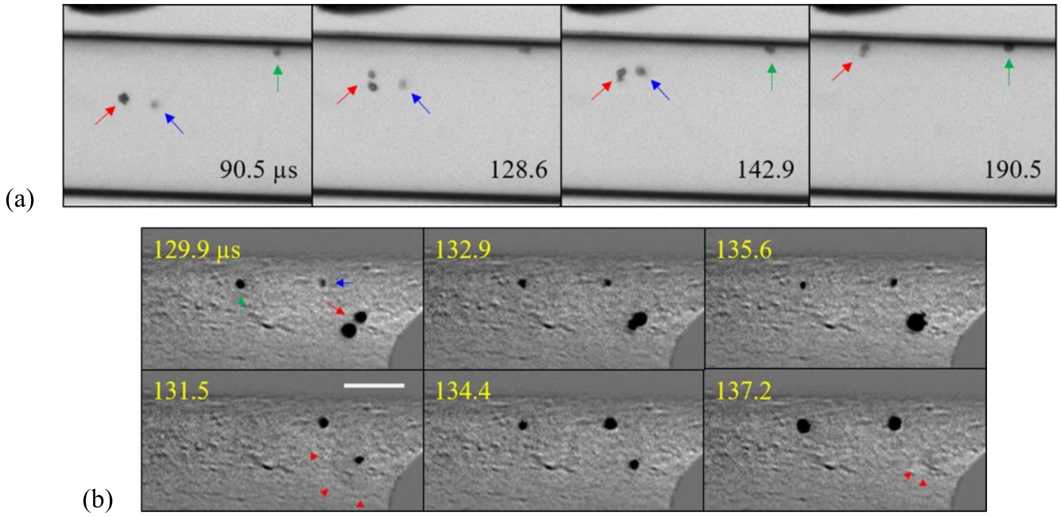

Fig. 2 High-speed imaging of multiple (3) microbubble cavitation events within the capillary, from (a) TV perspective at 210,000 fps, with scale given by capillary internal diameter of 500 μm and (b) SV perspective, at 10 million fps, with the scale bar: 150 μm (although this does not represent physical size, as imaging is slight defocused [1]). The tip of the needle hydrophone is apparent to the top left of (a), and bottom right, (b).

II. Materials and Methods

The experimental arrangement is represented schematically in Fig. 1. A 500 μm internal diameter polycarbonate capillary (25 μm wall thickness, Paradigm Optics), was positioned at 45° to the propagation axis of a focused ultrasound transducer, horizontally across the focal region. The transducer (H-149, Sonic Concepts) geometrically focuses to 68 mm from the front face, and was mounted on a *xyz* manipulator within a tank measuring 420 × 438 × 220 mm^3 filled with degassed, de-ionised water. t = 0 μs is defined as initial excitation of the transducer, with the focused ultrasound propagating to the capillary, at t ≈ 60 μs.

Phials of SonoVue (Bracco) contrast agent were reconstituted daily, with samples diluted by a factor of ~ 1:80,000 in de-ioinsed water, prepared on an hourly basis. A syringe pump flowed samples through the capillary at a rate of 11 mL/hr.

A. Dual perspective high-speed imaging

A high-speed camera (Fastcam SA-Z 2100K), mounted vertically above the capillary (top-view, TV), records the interaction between a 200-cycle burst of 692 kHz focused ultrasound (~290 μs in duration), and microbubbles in the capillary at the time of incidence, at 210,000 frames per second (fps). Imaging was undertaken through a 5× long working distance lens (0.14 NA, Mitutoyo), with field-of-view (FOV) represented by the dotted rectangle, fig. 1, and spatial resolution of ~ 4.1 $\mu m pixel^{-1}$. A second high-speed camera (Shimadzu HPV-X2) images at 10 million fps over a duration of 25.6 μs from a side-view (SV) perspective, through a Monozoom 7 lens (Bausch & Lomb), with a FOV represented by the dashed rectangle. The SV perspective captures microbubble-cavitation response over limited durations of interest within the focused ultrasound burst, at high temporal resolution. Illumination was achieved with synchronous (to frame capture) 10 ns laser pulses, coupled to a liquid light guide and a collimator lens, revealing pressure fluctuations within the FOV, via refractive index variations.

B. Acoustic detection

The acoustic emissions from the microbubble cavitation activity were detected with a 0.2-mm PVdF needle hydrophone (Precisions Acoustics, UK) in the orientation depicted, fig. 1. The hydrophone system has sensitivity and phase calibration from 100 kHz to 20 MHz in 25-kHz increments (National Physical Laboratory). Voltage data from the needle hydrophone system were amplified by 25 dB (Precision Acoustics) and collected, for the duration of the focused ultrasound exposure, to an oscilloscope (MS07104 A, Agilent Tech.), at 4 GS/s.

Time domain data is presented with the impulse response of the needle hydrophone deconvolved from the voltage data, over a selected bandwidth of 2.4-20 MHz. This removes the f_0 of the focused ultrasound (and non-linear components up to $3f_0$), for revealing shock wave content and restoring an approximation of pressure values [5]. Frequency spectra are generated via application of a fast Fourier transform and Hanning window to the time interval presented, but deconvolved across the full calibration bandwidth of 100 kHz - 20 MHz, and thereby include the driving, as well as microbubble cavitation emission components.

III. Results and Analysis

A. High speed imaging and acoustic data

Fig. 2 (a, b) are selected images from high-speed sequences of microbubble-cavitation captured in response to the focused ultrasound burst, at PNP = 1.14 MPa. As reported [1], this consistently drives cavitation in the period-doubled $f_0/2$ shock-emission regime. For this particular experiment, cavitation from three microbubbles within the capillary is apparent, arrowed red, blue and green in the imaging from both perspectives, fig. 2 (a, b).

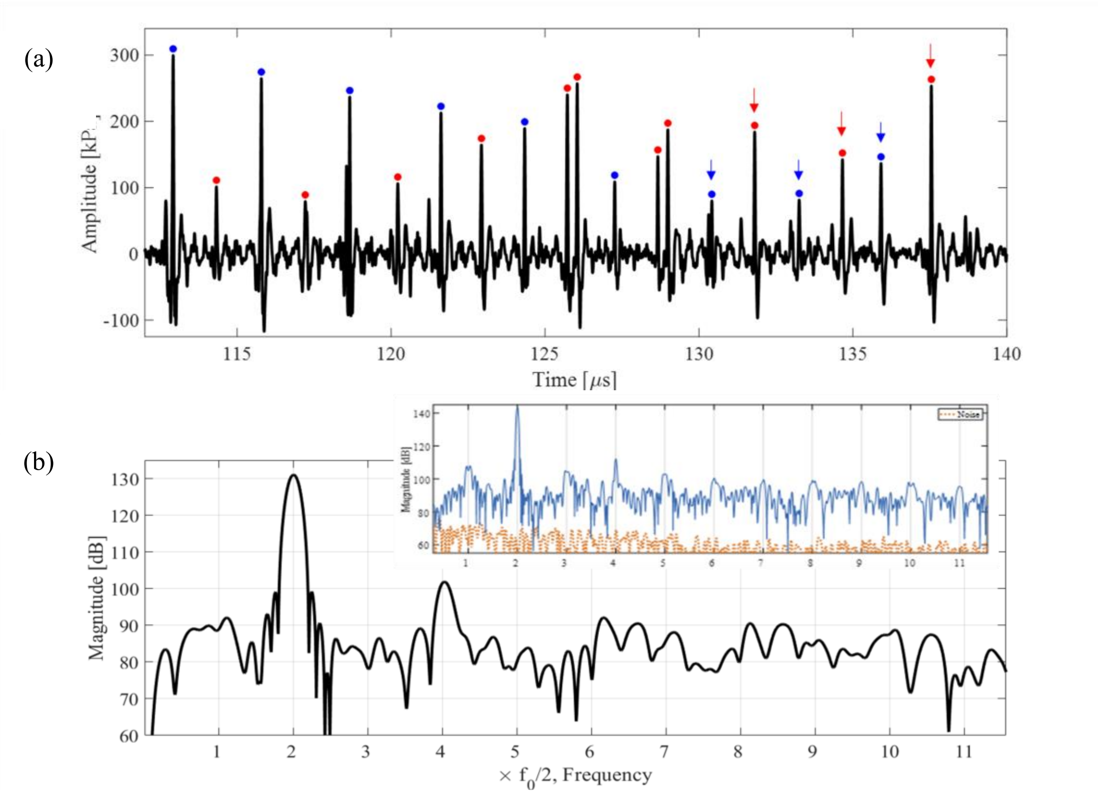

Fig. 3 (a) Filtered and deconvolved hydrophone time-domain data, of the combined emissions from the microbubble cavitation captured by Fig (2), and (b) its spectrum, revealing suppression of $nf_0/2$ peaks. Inset is spectrum of full emission signal collected over 200 cycle burst of focused ultrasound (blue) and instrumental noise (orange dot).

Arrows identifying bubble-collapse shockwaves apparent in the shadowgraphic imaging of fig. 2 (b), are colour-coded according to the cavitation source. Note, the microbubble-cavitation arrowed blue and green is less well focused in the TV imaging of fig. 2(a), as it is higher in the capillary, confirmed via SV imaging. TV imaging further suggests that the microbubble-cavitation arrowed red and blue may be coalescing at ~190 μs. SV imaging, however, confirms that the cavitation clouds remain separate from each other, certainly for the duration of acoustic data, presented fig. 3. In any case, the emissions from the clouds arrowed red and blue are expected to dominate the needle hydrophone data, as the cloud arrowed green is ~ 500 μm downstream of the needle tip location.

Fig. 3 (a) represents the filtered and deconvolved needle hydrophone data collected up to and including the SV high-speed imaging data. Shock waves from identifiable source microbubble-cavitation clouds, are colour-coded with a dot, with the specific shock waves imaged in fig. 2 (b), similarly arrowed in fig. 3 (a). The spectrum for the combined emission signal over the duration presented in fig. 3 (b), with the inset representing the spectrum single collected over the entire burst of focused ultrasound.

B. *Spectral windowing of the combined emission*

In [4], we outlined a simple analytical approach to analysing the combined emissions from two driven cavitation clouds. In that paper, experimental data was achieved via laser-nucleation, [6], of two clouds driven by focused ultrasound in the $f_0/2$ shock-emission regime. The collapse response of the clouds was in-phase, however they were positioned one wavelength apart, with respect to the sensing tip of the needle hydrophone detector. In the data presented here, the two microbubble cavitation clouds (identified red and blue) are effectively the same distance from the needle tip, but oscillating out of phase. The effect of apparent f_0 shock waves in the combined emissions, as detected by the needle, is therefore equivalent.

The synthetic bubble-collapse shockwave signal (ie, reconstructed with simulated bubble collapse shock wave profiles, [1, 3, 4]), is considered as the sum of the synthetic signals from the red and blue clouds of the data presented, in isolation of each other. As both clouds are responding in the $f_0/2$ regime, the emissions from the cloud arrowed blue ($x^b_{sw}(t)$) can be approximated in term for the emissions from the cloud arrowed red, (x^r_{sw}) as;

$$x^b_{sw}(t) \approx r.\ x^r_{sw}\ (t + \tau) \tag{1}$$

where r is the average ratio of peak-positive pressure amplitudes measured from the needle hydrophone data; $r = 0.85 \pm 0.74$ (± standard deviation) and τ the average difference in the detection time from each bubble-cloud; $\tau = 1.47 \pm 0.11$ μs (comparing to $1/f_0$ of the 692 kHz driving = 1.45 μs). The Fourier transform, $X^b_{sw}(f)$, of $x^b_{sw}(t)$ can thus be expressed in terms of the magnitude of the synthetic shock wave spectrum from the red cloud, as;

$$|X^b_{sw}(f)| \approx |1 + r \, . \, \cos(2\pi f\tau)| \, . \, |X^r_{sw}(f)| \quad (2)$$

Where $X_{sw}(f) = X^b_{sw}(f) + X^r_{sw}(f)$, and the $|1 + r \, . \, \cos(2\pi f\tau)|$ term acts as a periodic windowing function to the magnitude of the red cloud, to obtain the magnitude of the spectrum of the blue cloud. Here τ determines the spacing of the window suppressions (and therefore the frequency values that will be suppressed), with r determining the degree of suppression. Application to the data of fig. 3(a), yields fig. 4 where the blue curve is the window function imposed to the spectrum of the red cloud (red dot), to obtain the spectrum of the combined bubble-cloud emissions (solid red).

Fig. 4 indicates suppression at frequency values just less than $nf_0/2$ for **odd** values of n. The spectrum of the combined emission signal detected experimentally by the needle hydrophone, fig. 2(b), displays magnitude minima at similar frequency values. The degree of suppression is variable however, due to the high standard deviation associated with the value of r.

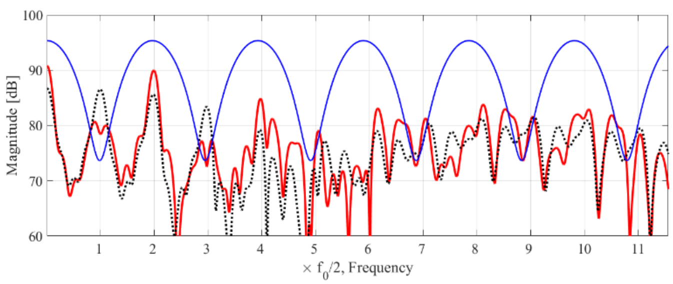

Fig. 4 Analysis of the spectrum of the combined emissions, in terms of the spectral window (blue) applied to the synthetic shock wave siganl of the cloud arrowed red in fig. 2.

IV. Discussion

In this proceeding we demonstrate spectral peak suppression in the combined acoustic emissions from microbubble cavitating under focused ultrasound. In the sample experimental data provided, two microbubble cavitation clouds respond in the $f_0/2$ shock wave emission regime, dictated by the PNP of the driving. Out-of-phase shock-emission, however, leads to apparent f_0 detection at the (single element) needle hydrophone detector tip. The spectrum of the combined emissions, over a limited duration, reveals subharmonic spectral peak suppression at circa $nf_0/2$, confirmed by an analytical expression of a window function, in terms of the emissions from one of the clouds considered separately.

We emphasize that the suppression occurs only over a limited time duration, within the 200-cycle burst of focused ultrasound. The spectrum of the signal collected over entire burst, inset to fig. 2(b), presents clear - but misshapen - peaks at $nf_0/2$, for $n = 1 - 11$ and higher, above broadband emissions and instrumental noise. Identification of the true source of the split peak at the $f_0/2$ subharmonic value, for example, would require synthetic reconstruction of the entire shock wave emission signal from both clouds, and identification of the source cloud behavior for each shock wave generated.

References

[1] J. H. Song, A. Moldovan, and P. Prentice, "Non-linear acoustic emissions from therapeutically driven contrast agent microbubbles," Ultrasound Med. Biol., vol. 8, pp. 2188-2204, 2019.

[2] W. Lauterborn and A. Koch, "Holographic observation of period-doubled and chaotic bubble oscillation in acoustic cavitation," Phys. Rev. A., vol. 35, pp. 1974-1976, 1987.

[3] J. H. Song, K. Johansen, and P. Prentice, "An analysis of the acoustic cavitation spectrum: The role of periodic shock waves," J. Acoust. Soc. Am., vol .140, pp. 2494-2505, 2016.

[4] J. H. Song, K. Johansen, and P. Prentice, "Covert cavitation: Spectral peak suppression in the acoutic emissions from spatially configured nucleations," J. Acoust. Soc. Am., vol. 141, EL216, 2017.

[5] K. Johansen, J. H. Song, K. Johnston, and P. Prentice, "Deconvolution of acoustically detected bubble-collapse shock waves," Ultrasonics, vol. 73, pp. 144-153, 2017.

[6] B. Gerold, S. Kotopoulis, C. McDougall, D. McGloin, M. Postema, and P. Prentice, "Laser-nucleated acoustic cavitation in focused ultrasound," Rev. Sci. Inst., vol 82, 044902, 2011.